J. Fluid Mech. (1980), *vol.* 100, *part* 1, *pp.* 111–128
Printed in Great Britain

Numerical analysis of unsteady secondary vortices generated by an impulsively started circular cylinder

By TA PHUOC LOC

Laboratoire d'Informatique pour la Mecanique et les Sciences de l'Ingenieur,
C.N.R.S., B.P. 30–91406–Orsay, France

(Received 10 August 1979 and in revised form 4 February 1980)

The mechanism of the creation of secondary vortices behind an impulsively started circular cylinder is analysed in this paper by a higher order of accuracy numerical method. This is a combination of second-order and fourth-order compact finite difference schemes to resolve complete unsteady Navier–Stokes equations. The fourth-order compact scheme is used to calculate the Poisson equation of the stream function and the second-order alternating direction implicit scheme to resolve the vorticity transport equation.

In particular, the growth of primary and secondary vortices with time is analysed for Reynolds numbers equal to 300, 550 and 1000. A single secondary vortex first appears at a Reynolds number equal to 300 on the surface of the cylinder. At $R = 550$, this creation is found numerically at dimensionless time t about 2·85, and this single secondary vortex is transformed into a pair of secondary vortices at t about 5. For $R = 1000$, two single vortices can be observed at t about 2·5, one near the separation point and another more important, easily identified in flow structure. These secondary vortices are transformed into a pair of secondary vortices at t about 4·5.

A numerical analysis of the influence of the grid systems and the time step is also given. All numerical results presented here are compared with experimental visualizations. The comparison is found satisfactory.

1. Introduction

Theoretical works on the problem of viscous flow past a circular cylinder, which is started impulsively from rest with constant velocity, fall into two main classes.

First, the flow for small times, before the appearance of the wake, may be studied using boundary-layer theory. Blasius (1908), Goldstein & Rosenhead (1936), Schuh (1953), Wundt (1955) and Watson (1955) have all considered this problem as the limiting case of infinite Reynolds number. Wang (1967) and Collins & Dennis (1973*a*, *b*) have extended the work to finite but high values of Reynolds numbers. The results however only indicate the flow structure for small times after starting.

The second class is that of purely numerical solutions of the Navier–Stokes equations and these are, on the whole, valid for 'any' value of the Reynolds number. Thom (1933) gave the first numerical solution of steady Navier–Stokes equations corresponding to the viscous flow around a circular cylinder. The unsteady flow was first studied by Payne (1958) for Reynolds equal to 40 and 100. Kawaguti & Jain (1966), Son & Hanratty (1969), Jain & Rao (1969), Thoman & Szewczyk (1969),

0022–1120/80/4532–2030 $02.00

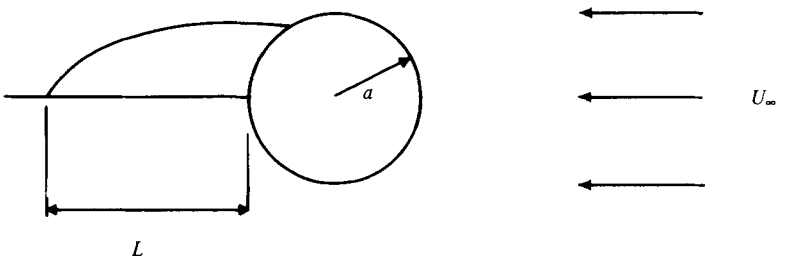

FIGURE 1. Schematic diagrams of the problem.

Dennis & Staniforth (1971), Collins & Dennis (1973*a*, *b*), Patel (1976) and Daube & Ta Phuoc Loc (1978) have investigated this problem for different Reynolds numbers. The common points of interest of these works are the development of the primary unsteady wake length behind the cylinder, and the evolution in time of the drag coefficient and the separation angle.

Besides these theoretical and numerical investigations, some experimental visualizations have been described by Honji & Taneda (1969), Taneda (1972) and recently by Coutanceau & Bouard (1977, 1979). A number of properties of the development of the unsteady wake have been studied and, in particular, the length of the pair of standing eddies formed behind the cylinder and the separation angle have been measured as a function of time for various values of R. The delicate problem of the formation of the secondary vortices has been also analysed.

If the comparison between experimental data and previous numerical results has in general shown agreement for Reynolds numbers up to 100, a discrepancy exists for greater Reynolds numbers, especially on the appearance of secondary vortices.

One of the objects of the present paper is to give a higher-order accurate numerical treatment for the analysis of the secondary vortices for Reynolds numbers equal to 300, 550 and 1000. Numerical results presented here are compared with experimental visualizations, and the agreement is found to be satisfactory.

Finally, this study shows that the divergence form of the transport equation of the vorticity is recommended in this problem for high Reynolds numbers.

2. Equations of motion and boundary conditions

Let us consider the unsteady laminar flow of a viscous incompressible fluid past a circular cylinder of radius a with a constant velocity U_∞ (see figure 1).

The unsteady Navier–Stokes equations in polar co-ordinates with stream-function and vorticity-dependent variables are

$$\frac{\partial \tilde{\omega}}{\partial \tilde{t}} - \frac{1}{\tilde{r}}\left(\frac{\partial}{\partial \tilde{r}}\left(\tilde{\omega}\frac{\partial \tilde{\psi}}{\partial \theta}\right) - \frac{\partial}{\partial \theta}\left(\tilde{\omega}\frac{\partial \tilde{\psi}}{\partial \tilde{r}}\right)\right) = \nu \nabla^2 \tilde{\omega}, \tag{1}$$

$$\tilde{\omega} = \nabla^2 \tilde{\psi} \tag{2}$$

and

$$\nabla^2 = \frac{\partial^2}{\partial \tilde{r}^2} + \frac{1}{\tilde{r}}\frac{\partial}{\partial \tilde{r}} + \frac{1}{\tilde{r}^2}\frac{\partial^2}{\partial \theta^2},$$

where $(\tilde{r}, \theta)$ are the polar co-ordinates, ν the kinematic viscosity, $\tilde{t}$ the time.

The variables $\tilde{\psi}$ and $\tilde{\omega}$ are defined by

$$\tilde{u} = -\frac{1}{\tilde{r}}\frac{\partial \tilde{\psi}}{\partial \theta}, \quad \tilde{v} = \frac{\partial \tilde{\psi}}{\partial \tilde{r}}, \quad \tilde{\omega} = \frac{1}{\tilde{r}}\left(\frac{\partial}{\partial \tilde{r}}(\tilde{v}\tilde{r}) - \frac{\partial \tilde{u}}{\partial \theta}\right).$$

If we write

$$\tilde{r} = ae^{\pi\xi}, \; \theta = \pi\eta, \; t = U_\infty \tilde{t}/a,$$

$$R = \frac{2U_\infty a}{\nu}, \quad \psi = \frac{\tilde{\psi}}{U_\infty a}, \quad \omega = \frac{\tilde{\omega} a}{U_\infty},$$

equations (1) and (2) can be written in dimensionless form

$$\frac{R}{2}\left(g(\xi,\eta)\frac{\partial \omega}{\partial t} + \frac{\partial}{\partial \eta}\left(\frac{\partial \psi}{\partial \xi}\omega\right) - \frac{\partial}{\partial \xi}\left(\frac{\partial \psi}{\partial \eta}\omega\right)\right) = \nabla^2 \omega, \tag{3}$$

$$\nabla^2 \psi = g(\xi,\eta)\,\omega, \tag{4}$$

with

$$\nabla^2 = \frac{\partial^2}{\partial \xi^2} + \frac{\partial^2}{\partial \eta^2} \quad \text{and} \quad g(\xi,\eta) = \pi^2 e^{2\pi\xi}.$$

To complete the system (3), (4), boundary conditions given by the physical problem are:

(i) no slip condition on the surface of the cylinder;

(ii) potential flow at infinity.

These conditions can be written in stream function and vorticity formulation as:

$$t \geqslant 0, \quad \left\{ \begin{array}{l} \psi = \dfrac{\partial \psi}{\partial \xi} = 0, \\ \text{No condition for } \omega, \end{array} \right\} \quad \xi = 0; \tag{5}$$

$$t \geqslant 0, \quad \left\{ \begin{array}{l} \psi = 2\sinh \pi\xi \sin \pi\eta, \\ \omega = 0, \end{array} \right\} \quad \xi \to \infty. \tag{6}$$

Equation (4) also gives

$$\frac{\partial^2 \psi}{\partial \xi^2} = g(\xi,\eta)\,\omega \quad \text{for} \quad \xi = 0; \tag{7}$$

this condition is necessary in the fourth-order compact numerical algorithm and allows us to determine the boundary condition for ω on the surface of the cylinder.

3. Numerical method

The method used is a combination of two numerical schemes, a fourth-order compact method for the resolution of the Poisson equation of stream function, and a second-order one for the calculation of the vorticity transport equation. This so-called combined method has been recently proposed by Ta Phuoc Loc & Daube (1977).

3.1. *Outlines of the compact fourth-order scheme*

It is a compact Hermitian finite-difference scheme. The fourth-order accuracy is achieved with a three-point approximation and by the introduction of the first and second derivatives of the unknown variables as the new unknowns of the problem. This technique has been proposed by Collatz (1966) and Kreiss (see Orszag &

Israeli 1974) and developed recently by Hirsh (1975) in the resolution of some problems of fluid mechanics.

Let us call h the spatial step of discretization, and f_i, f'_i and f''_i the values of the function f and its first and second derivatives at node i. The following tridiagonal relations can be written:

$$f'_{i-1}+4f'_i+f'_{i+1}=\frac{3}{h}(f_{i+1}-f_{i-1})+O(h^4), \tag{8}$$

$$f''_{i-1}+10f''_i+f''_{i+1}=\frac{12}{h^2}(f_{i+1}-2f_i+f_{i-1})+O(h^4). \tag{9}$$

It appears, consequently, that one must impose boundary conditions not only for the unknown f, but also for its first and second derivatives. Therefore, if N is the number of the grid nodes, we usually have $3N$ equations for $3N$ unknowns to be resolved, when trying to solve a second-order differential equation.

3.2. *Resolution of the Poisson equation of the stream function*

The compact higher-order method is chosen for the calculation of the Poisson equation. The finite-difference equations obtained by discretization of the equation (4) and the tridiagonal relations (8) and (9) are resolved by a technique derived from the alternating direction implicit (A.D.I.) scheme.

Besides higher accuracy, another advantage of this method over the classical second-order methods lies in the possibility of simultaneously taking into account the boundary conditions on ψ and ψ' which are data of the physical problem.

In equation (4) only ψ and its second derivative appear. Consequently, by using relation (9) we can write for each step of the $(k+1)$th iteration of the A.D.I. technique, the following system:

$$\lambda_{kh}\psi_{ij}^{k+\frac{1}{2}}-\left(\frac{\partial^2\psi}{\partial\eta^2}\right)_{ij}^{k+\frac{1}{2}}=-g_{ij}\omega_{ij}^{n+1}+\left(\frac{\partial^2\psi}{\partial\xi^2}\right)_{ij}^{k}+\lambda_{kh}\psi_{ij}^{k}, \tag{10}$$

$$\frac{12}{(\Delta\eta)^2}(\psi_{i\,j+1}^{k+\frac{1}{2}}-2\psi_{ij}^{k+\frac{1}{2}}+\psi_{i\,j+1}^{k+\frac{1}{2}})-\left(\left(\frac{\partial^2\psi}{\partial\eta^2}\right)_{i\,j-1}^{k+\frac{1}{2}}+10\left(\frac{\partial^2\psi}{\partial\eta^2}\right)_{ij}^{k+\frac{1}{2}}+\left(\frac{\partial^2\psi}{\partial\eta^2}\right)_{i\,j+1}^{k+\frac{1}{2}}\right)=0 \tag{11}$$

and

$$\lambda_{kv}\psi_{ij}^{k+1}-\left(\frac{\partial^2\psi}{\partial\xi^2}\right)_{ij}^{k+1}=-g_{ij}\omega_{ij}^{n+1}+\left(\frac{\partial^2\psi}{\partial\eta^2}\right)_{ij}^{k+\frac{1}{2}}+\lambda_{kv}\psi_{ij}^{k+\frac{1}{2}}, \tag{12}$$

$$\frac{12}{(\Delta\xi)^2}(\psi_{i-1\,j}^{k+1}-2\psi_{ij}^{k+1}+\psi_{i+1\,j}^{k+1})-\left(\left(\frac{\partial^2\psi}{\partial\xi^2}\right)_{i-1\,j}^{k+1}+10\left(\frac{\partial^2\psi}{\partial\xi^2}\right)_{ij}^{k+1}+\left(\frac{\partial^2\psi}{\partial\xi^2}\right)_{i+1\,j}^{k+1}\right)=0, \tag{13}$$

where λ_{kh} and λ_{kv} are optimum coefficients of relaxation of the A.D.I. technique.

Boundary conditions are very simple since ψ is known on the boundary and its second derivatives can be expressed in terms of vorticity function by equation (7).

For each line i = constant or j = constant, we have to solve a $2N\times 2N$ blocks tridiagonal system which, in fact, easily reduces to a $N\times N$ tridiagonal system solved by the factorization algorithm.

Once the new values of ψ_{ij}^{n+1} of the stream function have been computed, by the tridiagonal relation (8), first derivatives $(\partial\psi/\partial\xi)_{ij}^{n+1}$ and $(\partial\psi/\partial\eta)_{ij}^{n+1}$ are calculated on each line i and j.

3.3. *Resolution of the vorticity transport equation*

A second-order accurate scheme has been chosen to solve this equation. This choice is motivated by the research of simplicity in checking boundary conditions and by the possibility to use the divergence form of Navier–Stokes equations and the first- or second-order upwind approximation of transport terms.

Also, it is important to note that, whatever the method used, boundary conditions for ω are always determined from the knowledge of ψ and its derivatives. A 'better accuracy' for the computation of ψ is then needed.

As for the treatment of the Poisson equation of the stream function, the A.D.I. algorithm has been used for the vorticity transport equation. Each dimensionless time-step Δt is decomposed in two successive half-step with a second-order accuracy.

Let n be the index of the nth time-step, we have the following expression:

$$R\frac{g_{ij}}{\Delta t}\omega_{ij}^{n+\frac{1}{2}} - \frac{\omega_{ij+1}^{n+\frac{1}{2}} - 2\omega_{ij}^{n+\frac{1}{2}} + \omega_{ij-1}^{n+\frac{1}{2}}}{(\Delta\eta)^2} + \frac{R}{4}\frac{(u\omega)_{ij+1}^{n+\frac{1}{2}} - (u\omega)_{ij-1}^{n+\frac{1}{2}}}{\Delta\eta}$$

$$= R\frac{g_{ij}}{\Delta t}\omega_{ij}^{n} + \frac{\omega_{i+1j}^{n} - 2\omega_{ij}^{n} + \omega_{i-1j}^{n}}{(\Delta\xi)^2} - \frac{R}{4}\frac{(v\omega)_{i+1j}^{n} - (v\omega)_{i-1j}^{n}}{\Delta\xi} \tag{14}$$

and

$$R\frac{g_{ij}}{\Delta t}\omega_{ij}^{n+1} - \frac{\omega_{i+1j}^{n+1} - 2\omega_{ij}^{n+1} + \omega_{i-1j}^{n+1}}{(\Delta\xi)^2} + \frac{R}{4}\frac{(v\omega)_{i+1j}^{n+1} - (v\omega)_{i-1j}^{n+1}}{\Delta\xi}$$

$$= R\frac{g_{ij}}{\Delta t}\omega_{ij}^{n+\frac{1}{2}} + \frac{\omega_{ij+1}^{n+\frac{1}{2}} - 2\omega_{ij}^{n+\frac{1}{2}} + \omega_{ij-1}^{n+\frac{1}{2}}}{(\Delta\eta)^2} - \frac{R}{4}\frac{(u\omega)_{ij+1}^{n+\frac{1}{2}} - (u\omega)_{ij-1}^{n+\frac{1}{2}}}{\Delta\eta}. \tag{15}$$

Here u and v are the components of the velocity, calculated from the values of ψ at instant n. The total order of accuracy of this scheme is $O((\Delta\xi)^2, (\Delta\eta)^2, \Delta t)$.

A second-order approximation is used to determine the value of the vorticity at the boundary. From equation (4) we can write:

$$2g(0,\eta)\,\omega(0,\eta) + g(\Delta\xi,\eta)\,\omega(\Delta\xi,\eta) = \frac{6}{(\Delta\xi)^2}(\psi(0,\eta) - \psi(\Delta\xi,\eta)). \tag{16}$$

3.4. *Accuracy*

The accuracy of this method in the numerical calculation of Navier–Stokes equations has been studied by Ta Phuoc Loc & Daube (1978) and by Roux *et al.* (1979). Several external and internal test problems have been considered and a comparison has been made between present combined method and a complete fourth order method used by Hirsh (1975). It appears that in the driven cavity problem and in the analytical problem suggested by Pearson (1965), the combined method gives, for a same grid system, an accuracy comparable to that obtained with a complete fourth-order one. However, an important advantage of the present method is the possibility to avoid high-frequency oscillations of higher-order numerical method when solving high-Reynolds-numbers problems.

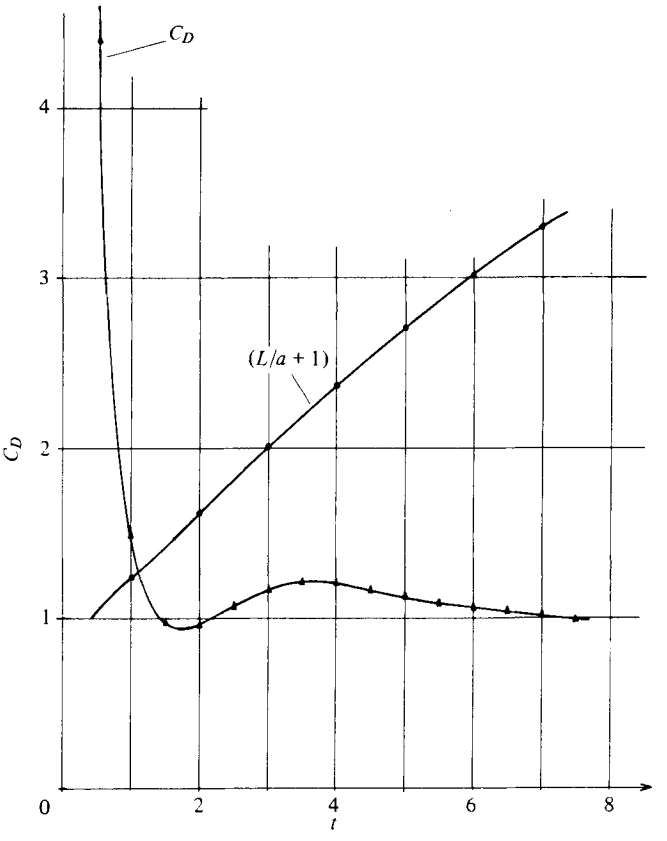

FIGURE 2. Evolution with time of the drag coefficient C_D and the main vortex length L for $R = 300$.

4. Results

The numerical calculations have been made on a UNIVAC 1110 computer. For each Reynolds number two formulations, divergence and convective forms, of the transport terms of the vorticity equation are considered. Results obtained on the evolution with time of the flow pattern, the drag coefficient, the distribution of vorticity at the cylinder surface are reported for Reynolds numbers equal to 300, 550, 1000. A comparison between experimental data and numerical results is also realized.

4.1. $R = 300$

For $R = 300$, a grid system of 41×41 nodes is adopted ($\Delta\eta = 1/40$; $\Delta\xi = 0{\cdot}954/40$). The dimensionless time-step is taken equal to 0·05. The C.P.U. time for each time-step is equal about 0·95 s.

In figure 2, the results of time evolution of the length of the main vortex and the drag coefficient are shown. The radial velocity on the symmetry axis behind the cylinder presented in figure 3 is to be compared with experimental measures. We can note the existence of values of the velocity modulus greater than 1 in the primary vortex. The distribution of the vorticity at the cylinder surface, given in figure 4 permits to determine the moment of the appearance of a secondary vortex which is

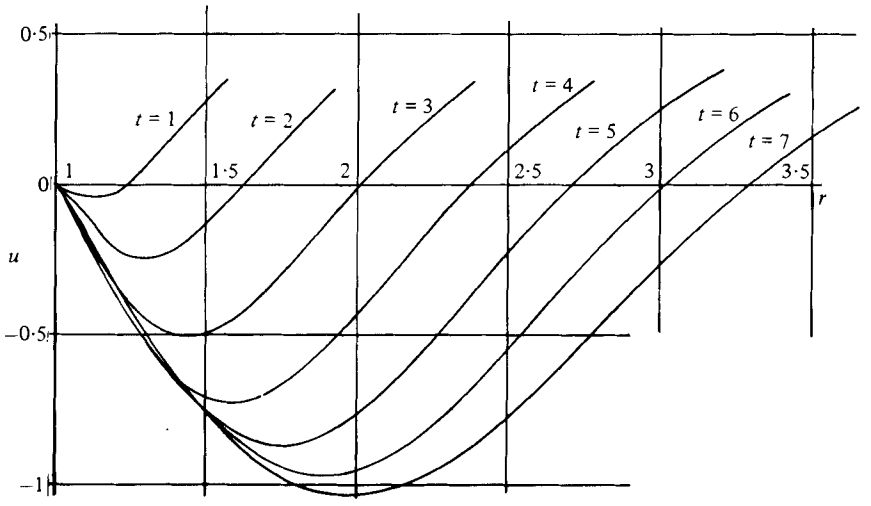

FIGURE 3. Evolution with time of the radial velocity on the symmetry axis behind the cylinder for $R = 300$.

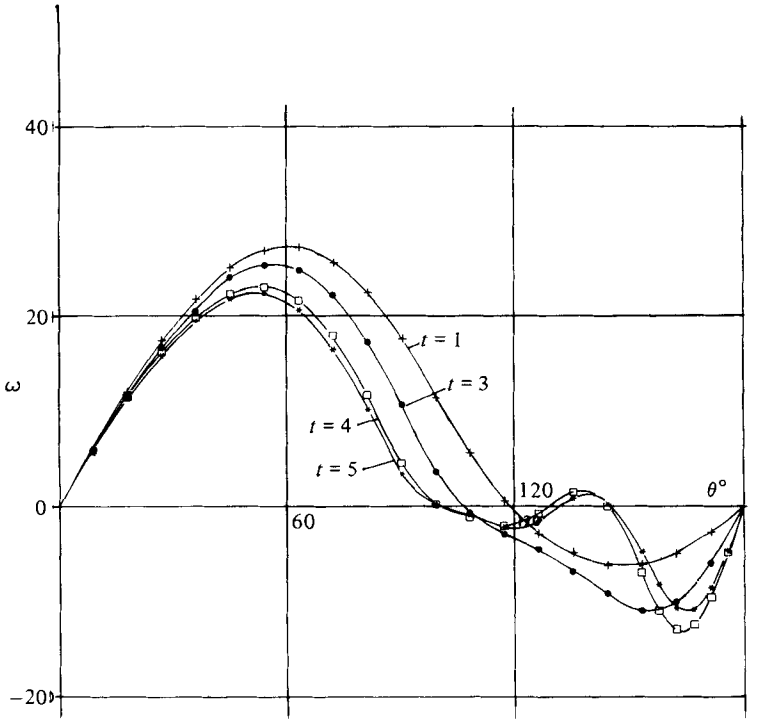

FIGURE 4. Evolution with time of the vorticity distribution at the cylinder surface for $R = 300$.

about $t = 3{\cdot}5$. The development of the flow structure with time is shown in figure 5. A comparison with experimental visualization, for $t = 5$, of the flow pattern obtained by numerical treatment is given in figure 6 (plate 1). At this Reynolds number only a single secondary vortex is observed.

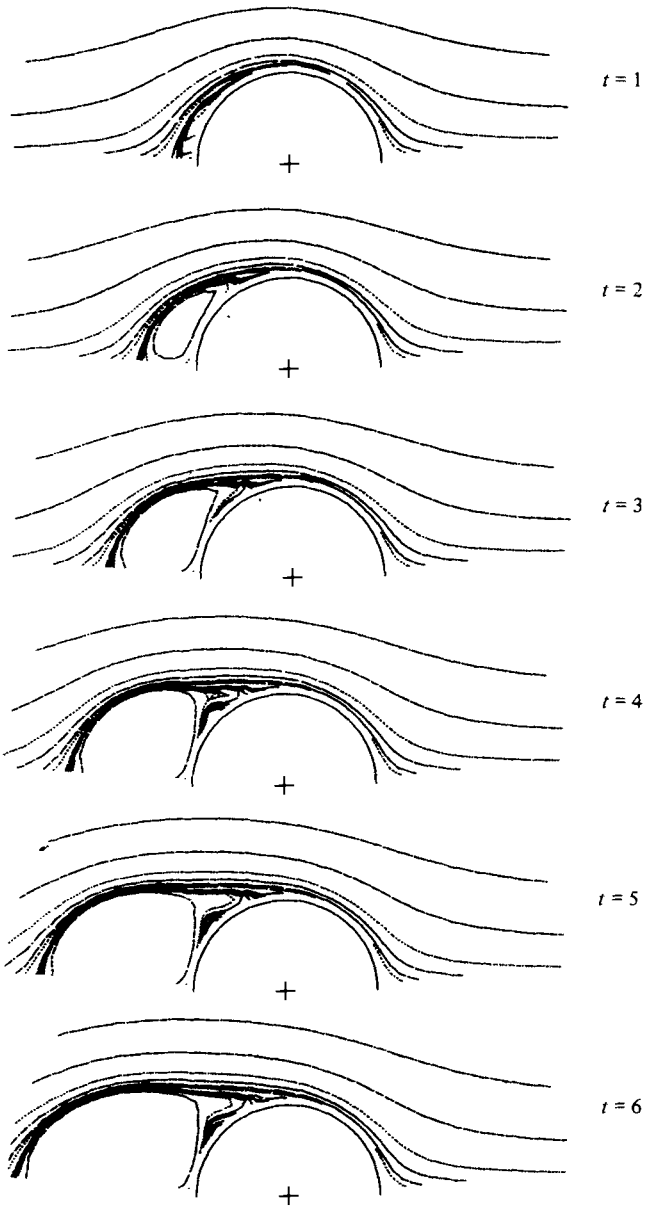

FIGURE 5. Streamlines showing the evolution with time of the flow pattern for $R = 300$.

4.2. $R = 550$

For this Reynolds number two experimental visualizations have been realized, by Honji & Taneda (1969), and recently by Coutanceau & Bouard (1979). They have observed the presence of a pair of secondary vortices at t about 5.

Numerical results reported by Patel (1976), Collins & Dennis (1973*a*, *b*) and Son & Hanratty (1969) point out only the appearance of a single secondary vortex, and an

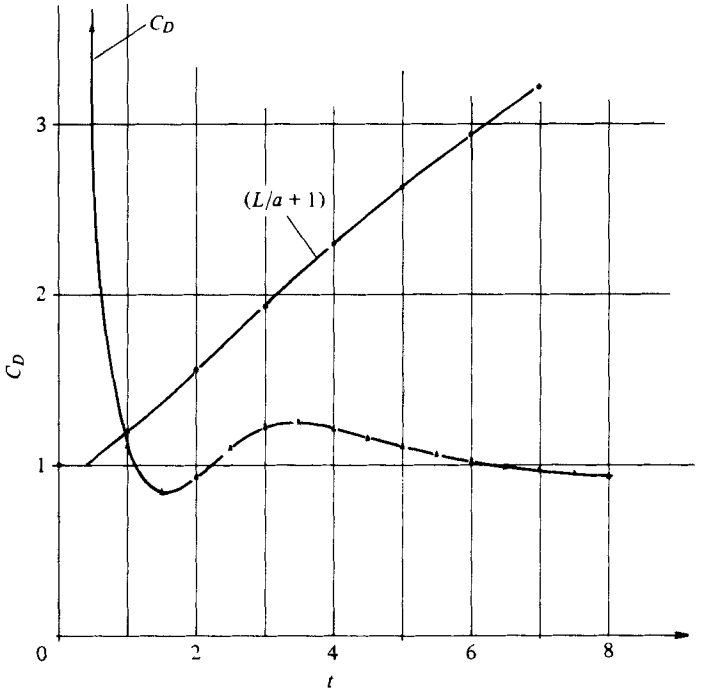

FIGURE 7. Evolution with time of the drag coefficient C_D and the main vortex length L for $R = 550$ with a grid system of 61×61 nodes.

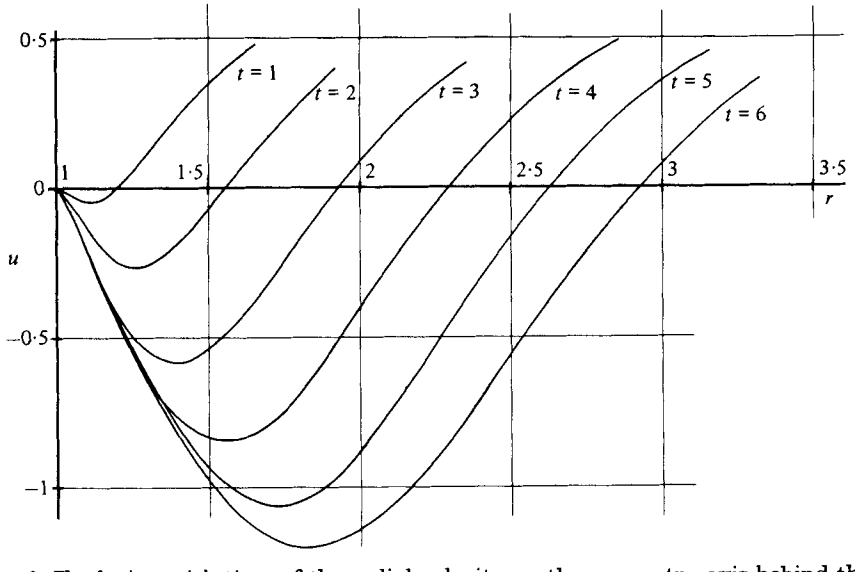

FIGURE 8. Evolution with time of the radial velocity on the symmetry axis behind the cylinder for $R = 550$ with a grid of 61×61 nodes.

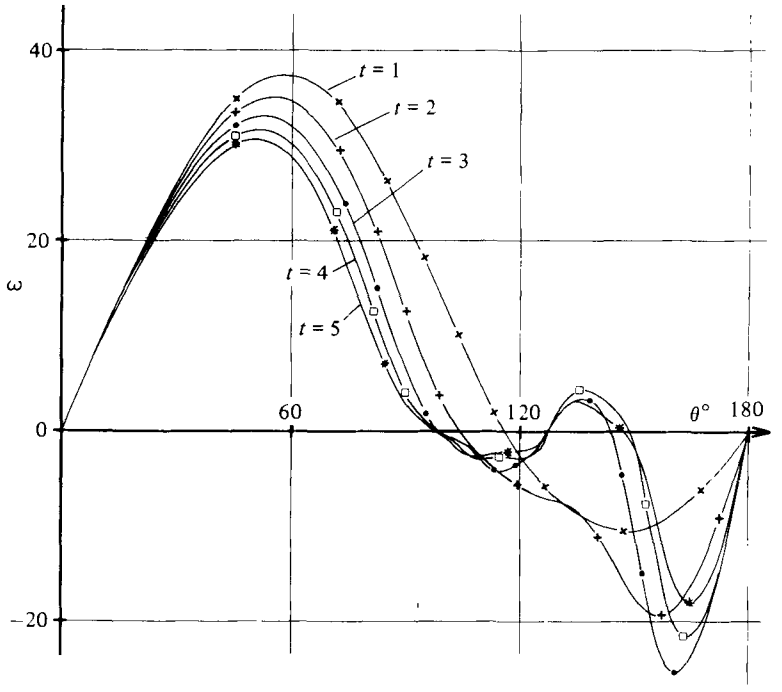

FIGURE 9. Evolution with time of the vorticity distribution at the cylinder surface for $R = 550$.

important discrepancy between experimental data and numerical results can be observed.

However, results presented in this paper can be compared with a reasonable agreement to experimental visualization.

The grid system of 61×61 nodes is used for this Reynolds number ($\Delta\eta = 1/60$; $\Delta\xi = 0{\cdot}954/60$). The time-step of 0·033 s is adopted. The time evolution of the length of the main vortex and of the drag coefficient is reported in figure 7. We can note that the time necessary to obtain the same value of the wake length is greater for $R = 550$ than for $R = 300$. The radial velocity on the symmetry axis behind the cylinder is shown in figure 8. We can note that the velocity modulus in the main vortex becomes more important and exceeds 1 at $t = 5$. The variation in time of the distribution of the vorticity at the cylinder surface described in figure 9 indicates that a single secondary vortex appears at $t = 2{\cdot}85$. The area of this single vortex increases with time and a pair of secondary vortices can be observed at $t = 5$ as shown in the figure 11. This phenomenon is not pointed out by previous authors in their numerical results. In figure 10 the development of the flow structure is given. A comparison between experimental visualization and present numerical results is shown in figure 11 (plate 2): the agreement is found to be close enough.

4.3. $R = 1000$

Because of stability conditions and for accuracy, a grid of 81×41 nodes is chosen, with a time step of 0·025 for this Reynolds number. The C.P.U. time for each time step is now equal to 1·90 s. The time evolution of the drag coefficient and the wake length is

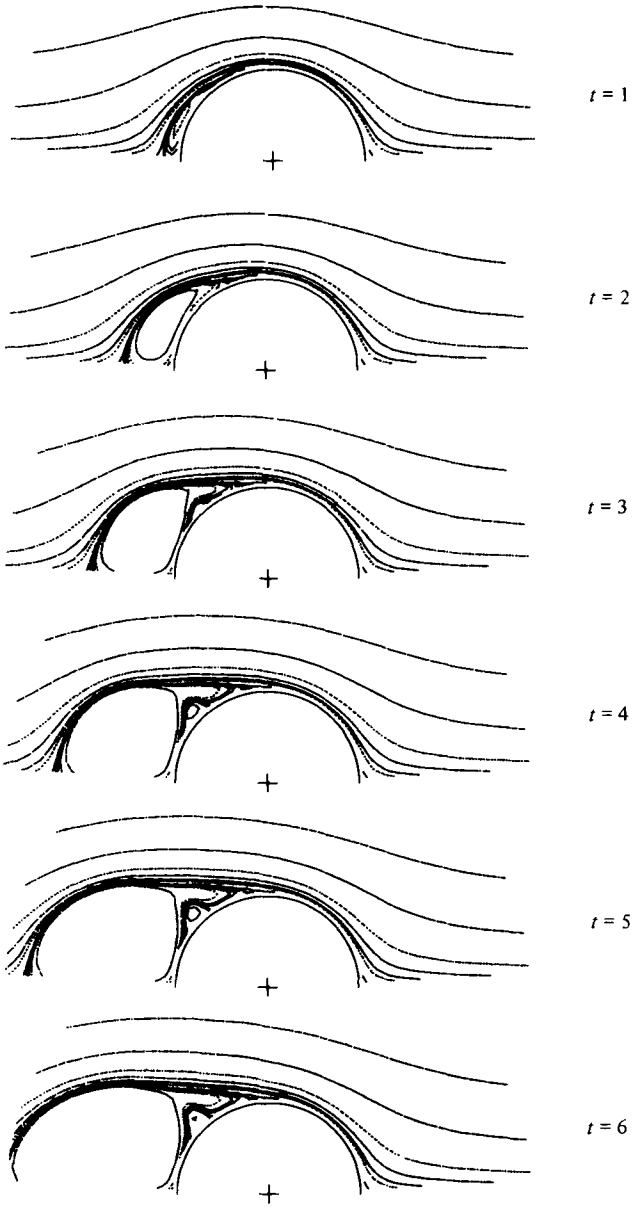

FIGURE 10. Streamlines. Evolution with time of the flow pattern for $R = 550$.

presented in figure 12. The time necessary to obtain the same value of wake length is greater for $R = 1000$ than for $R = 550$. This observation has also been pointed out experimentally by Coutanceau & Bouard (1979). The radial velocity on the symmetry axis behind the cylinder is given in figure 13 and can be compared to experimental measurements. The values of the velocity modulus greater than 1 can again be observed in the wake at t about 4.8. The repartition of the vorticity on the cylinder surface, permitting the determination of the moment of the appearance of a secondary vortex,

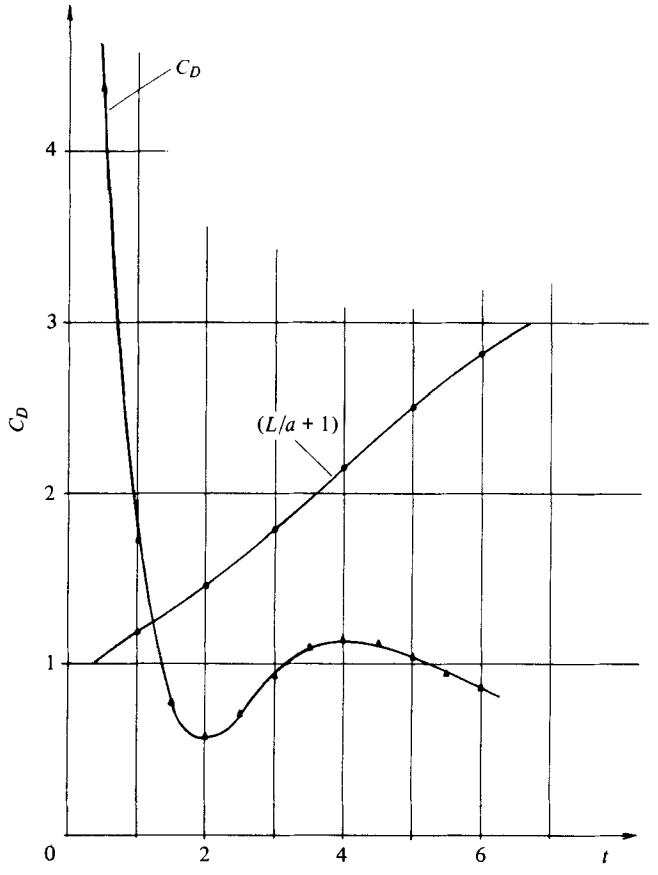

FIGURE 12. Evolution with time of the drag coefficient C_D and the main vortex length L for $R = 1000$.

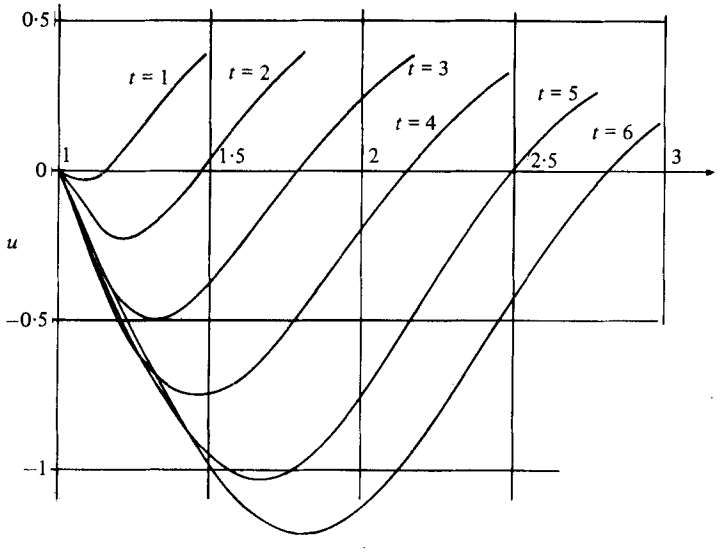

FIGURE 13. Evolution with time of the radial velocity on the symmetry axis behind the cylinder for $R = 1000$.

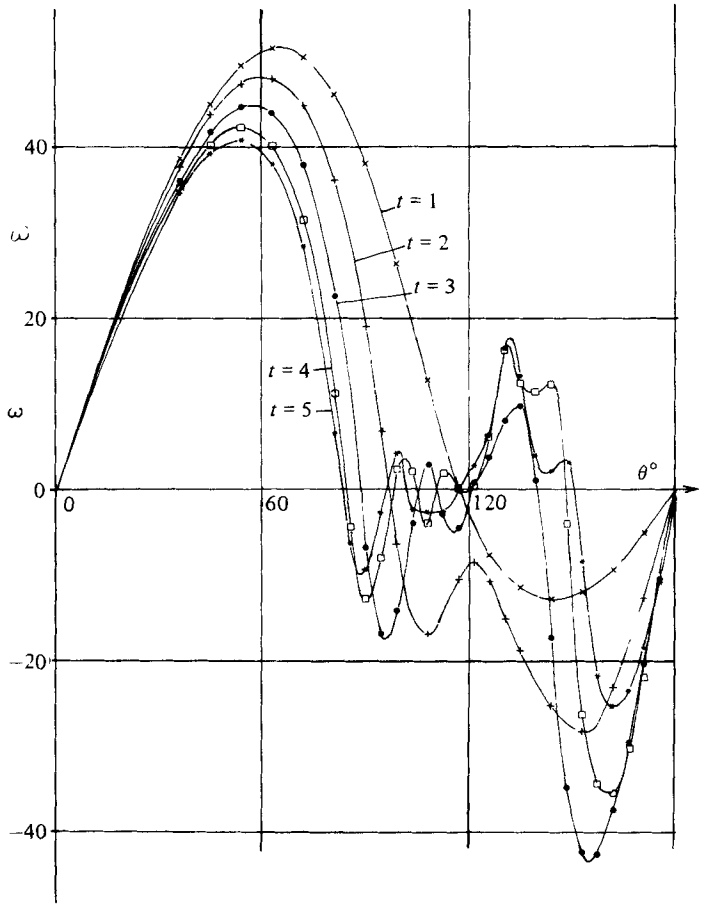

FIGURE 14. Evolution with time of the vorticity distribution at the cylinder surface for $R = 1000$.

is given in figure 14. At $t = 3$, we can observe two secondary vortices. The first one is localized near the separation point and the second one, of greater intensity and area, is identified easily in the flow pattern. These secondary vortices are transformed into a pair of secondary vortices with a small single vortex near the separation point at t equal about 4·5. This phenomenon has also been pointed out experimentally by Honji & Taneda (1969) and recently by Bouard & Coutanceau (1979, private communication). The development of the flow structure with time is described in figure 15. At $t = 5$ we can note the importance of the main pair of secondary vortices.

4.4. *Influence of the grid systems*

Three grid systems and three values of time-step are considered for the Reynolds number equal to 550. The relation (16) shows that the vorticity distribution on the cylinder surface depends strongly on the radial step discretization $\Delta\xi$.

The first calculation is made with a grid of 41×41 nodes ($\Delta\eta = 1/40$; $\Delta\xi = 0{\cdot}954/40$; $\Delta t = 0{\cdot}05$), the second one with a grid of 51×51 ($\Delta\eta = 1/50$; $\Delta\xi = 0{\cdot}954/50$; $\Delta t = 0{\cdot}04$) and the third one with a grid of 61×61 nodes ($\Delta\eta = 1/60$; $\Delta\xi = 0{\cdot}954/60$; $\Delta t = 0{\cdot}03$).

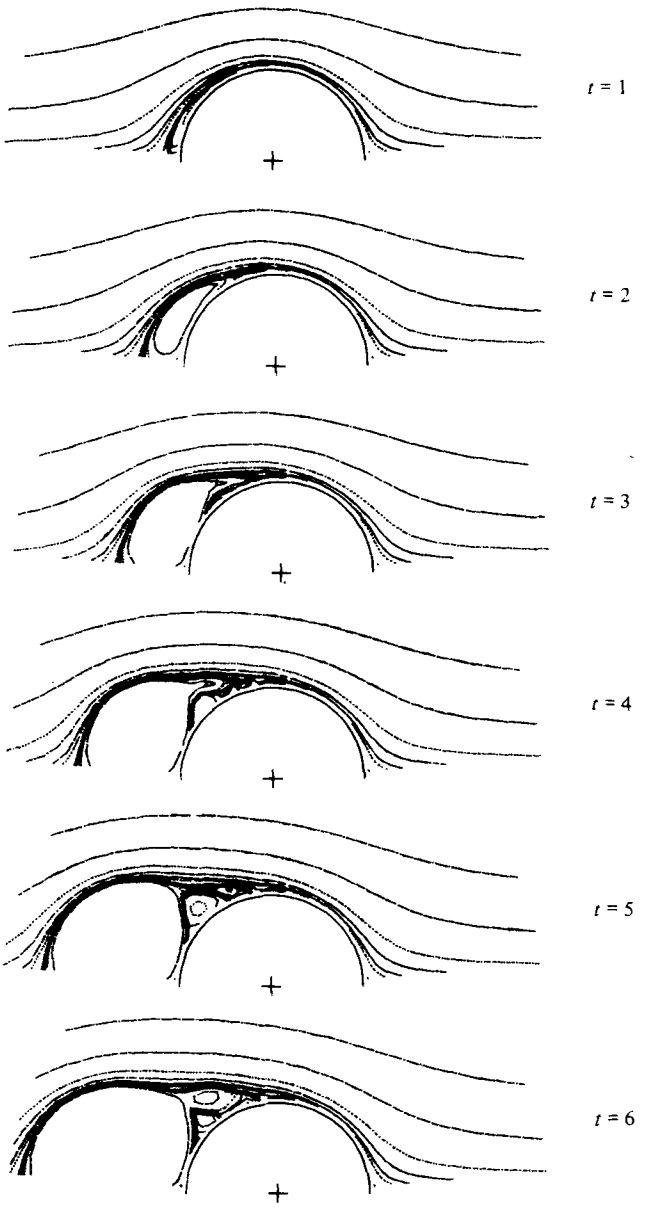

FIGURE 15. Streamlines. Evolution with time of the flow pattern for $R = 1000$.

If some difference is observed on the vorticity repartition on the cylinder surface and consequently on the drag coefficient, the flow structure changes slightly as shown in figure 11. We can note the appearance of secondary vortices at the same time in all cases. It is important to remark that the time step is different for each calculation.

In figures 16 and 17, the evolution of the drag coefficient, the length of the main vortex and the radial velocity on the symmetry axis are reported for these three grid systems. We can see that no important difference on the velocity and on the wake

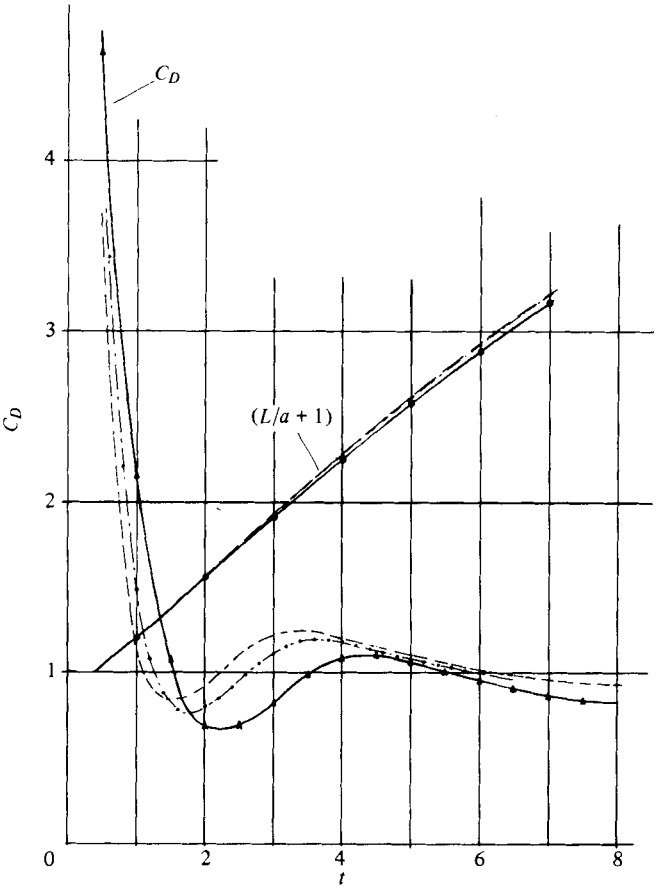

FIGURE 16. Influence of the grid systems and of the time step on the drag coefficient C_D and on the main vortex length L for $R = 550$ with various grid systems: ——, 41×41 nodes; – · – 51×51 nodes; – – –, 61×61 nodes.

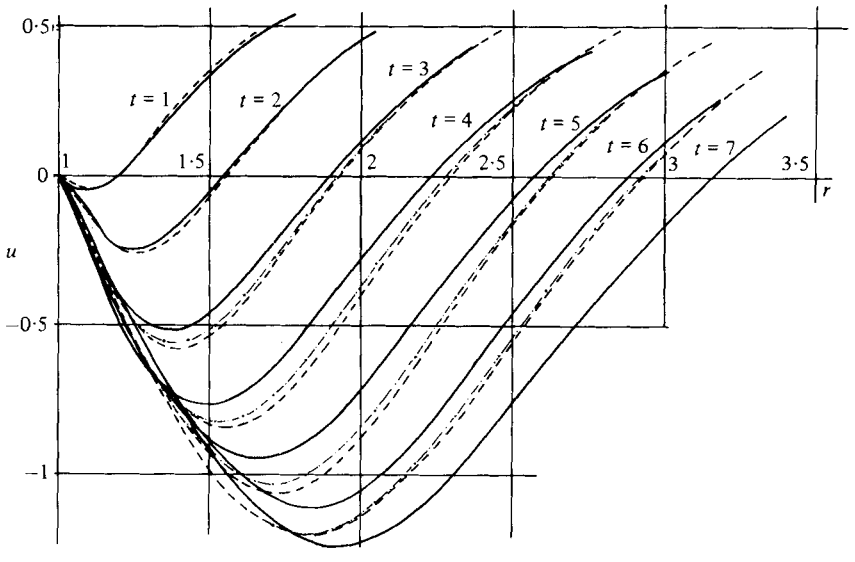

FIGURE 17. Influence of the grid systems and of the time step on the radial velocity on the symmetry axis behind the cylinder for $R = 550$. See figure 16 for an explanation of the curves.

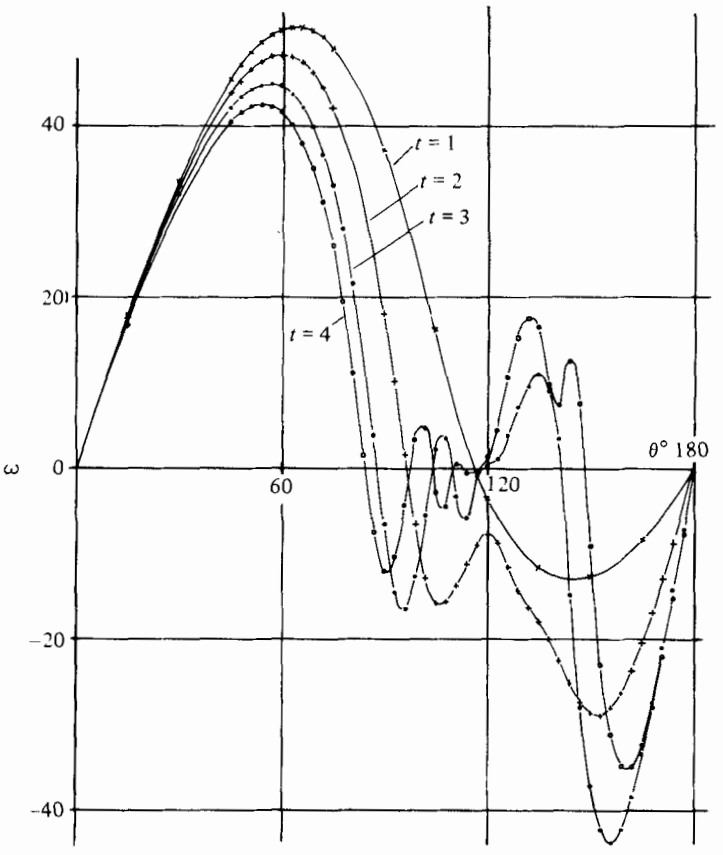

FIGURE 18. Evolution with time of the vorticity distribution at the cylinder surface for $R = 1000$ with a grid system of 61×61 nodes.

length is observed between the 51×51 nodes grid system and the 61×61 nodes one. The grid of 61×61 nodes can be considered as sufficient for Reynolds number of 550.

For Reynolds number equal to 1000, two grid systems are used (41×81 and 61×61). The relative importance of the spatial discretization in η and ξ directions is analysed. With a same value of $\Delta\xi = 0{\cdot}954/60$, two values of $\Delta\eta$ and Δt are considered ($\Delta\eta = /401$; $\Delta t = 0{\cdot}025$; $\Delta\eta = 1/60$; $\Delta t = 0{\cdot}0166$). The vorticity distribution on the cylinder surface, given in figure 18, shows a relative importance of $\Delta\eta$ discretization compared with $\Delta\xi$ discretization because of the relation (16). Results obtained with these two grid systems do not present any difference.

Finally, in figure 19, a comparison between numerical results obtained by divergence form or convective form of the transport terms of Navier–Stokes equations shows that it is better to use the divergence form rather than the convective form for high-Reynolds-number calculations.

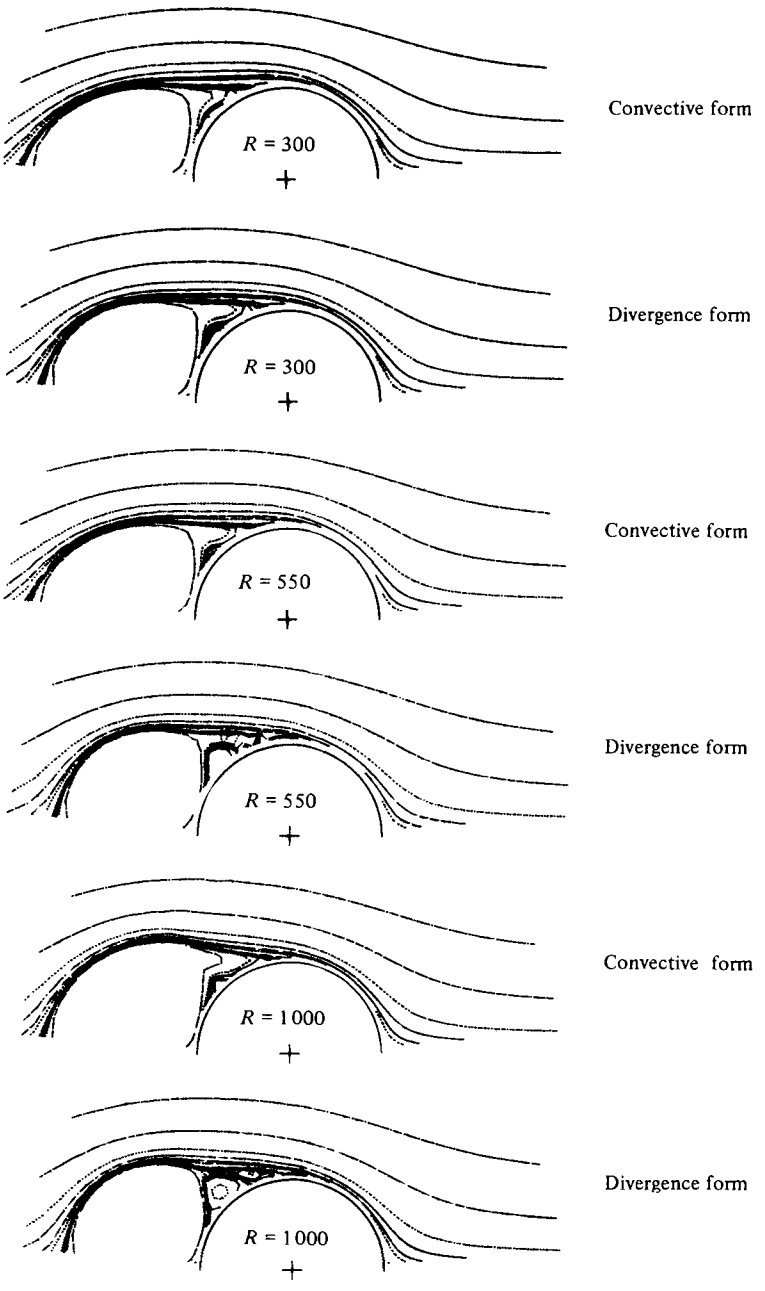

FIGURE 19. Comparison between numerical results given by convective and divergence forms of the transport terms of the vorticity equation.

5. Conclusion

The complex problem of unsteady viscous flow around a circular cylinder has been studied in detail in this paper. Some properties on the creation and the development of the primary and secondary vortices are made evident and are verified by experimental data.

Moreover, results presented here demonstrate, first, the utility of the use of the divergence form of the transport terms in the numerical integration of Navier–Stokes equations, secondly, the accuracy and the efficiency of the combined second- and fourth-order compact numerical method in unsteady flow analysis.

The author acknowledges the many helpful comments and suggestions of the referees.

REFERENCES

BLASIUS, H. 1908 *Z. angew. Math. Phys.* **56**, 1.

COLLATZ, L. 1966 *The Numerical Treatment of Differential Equations.* Springer.

COLLINS, W. M. & DENNIS, S. C. R. 1973*a* *Quart. J. Mech. Appl. Math.* **26**, 53.

COLLINS, W. M. & DENNIS, S. C. R. 1973*b* *J. Fluid Mech.* **60**, 105.

COUTANCEAU, M. & BOUARD, R. 1977 *J. Fluid Mech.* **79**, 257.

COUTANCEAU, M. & BOUARD, R. 1979 *C. R. Acad. Sci. Paris*, **288**, B45.

DAUBE, O. & TA PHUOC LOC 1978 *J. Méc.* **17**, 651.

DENNIS, S. C. R. & STANIFORTH, A. N. 1971 *Proc. 2nd Int. Conf. on Numerical Methods in Fluid Dynamics*, Lecture Notes in Physics, vol. 8, p. 343. Springer.

GOLDSTEIN, S. & ROSENHEAD, L. 1936 *Proc. Camb. Phil. Soc.* **32**, 392.

HIRSH, R. S. 1975 *J. Comp. Phys.* **19**, 90.

HONJI, H. & TANEDA, S. 1969 *J. Phys. Soc. Japan* **27**, 1668.

JAIN, P. C. & RAO, K. S. 1969 *Phys. Fluids Suppl.* **12**, II57.

KAWAGUTI, M. & JAIN, P. C. 1966 *J. Phys. Soc. Japan* **21**, 2055.

ORSZAG, S. A. & ISRAELI, M. 1974 *Ann. Rev. Fluid Mech.* **6**, 281.

PATEL, V. A. 1976 *Comp. & Fluids* **4**, 13.

PAYNE, R. B. 1958 *J. Fluid Mech.* **4**, 81.

PEARSON, C. E. 1965 *J. Fluid Mech.* **21**, 611.

ROUX, B., BONTOUX, P., TA PHUOC LOC & DAUBE, O. 1979 Approximation Methods for Navier–Stokes Problems, IUTAM-SYMPOSIUM Paderborn (W. Germany).

SCHUH, H. 1953 *Z. Flugwiss.* **1**, 122.

SON, J. S. & HANRATTY, T. J. 1969 *J. Fluid Mech.* **35**, 369.

TANEDA, S. 1972 *Recent Research on Unsteady Boundary Layers*, vol. 2 (ed. E. A. Eichelbrenner). Quebec Laval University.

TA PHUOC LOC & DAUBE, O. 1977 *C. R. Acad. Sci. Paris* **284**, A1241.

TA PHUOC LOC & DAUBE, O. 1978 *Special Session, Int. Conf. Numerical Methods in Laminar and Turbulent Flow, Swansea.*

THOM, A. 1933 *Proc. Roy. Soc.* A 141, 651.

THOMAN, D. C. and SZEWCZYK, A. A. 1969 *Phys. Fluids Suppl.* **12**, II76.

WANG, C. Y. 1967 *J. Math. Phys.* **46**, 195.

WATSON, E. J. 1955 *Proc. Roy. Soc.* A **231**, 104.

WUNDT, H. 1955 *Ing.-Arch. Berlin*, **23**, 212.

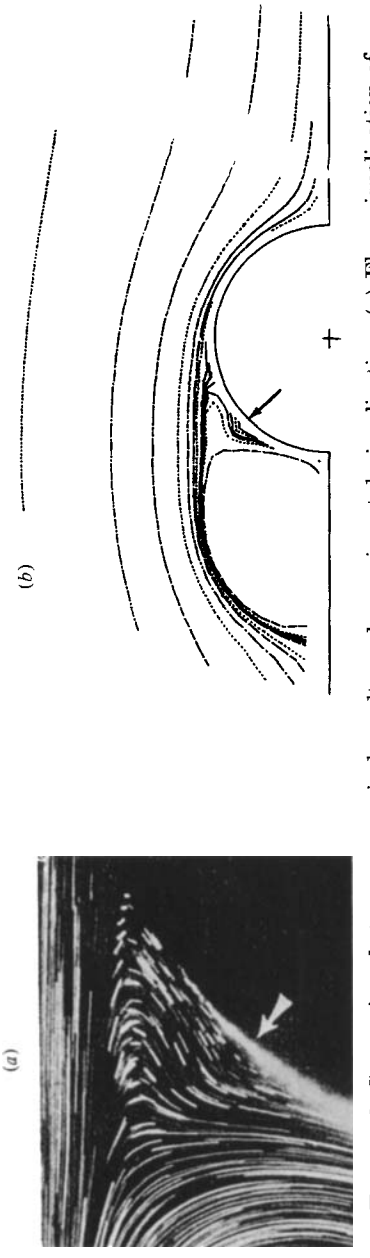

FIGURE 6. Comparison between numerical results and experimental visualization. (*a*) Flow visualization of Coutanceau & Bouard (1979), (*b*) numerical results.

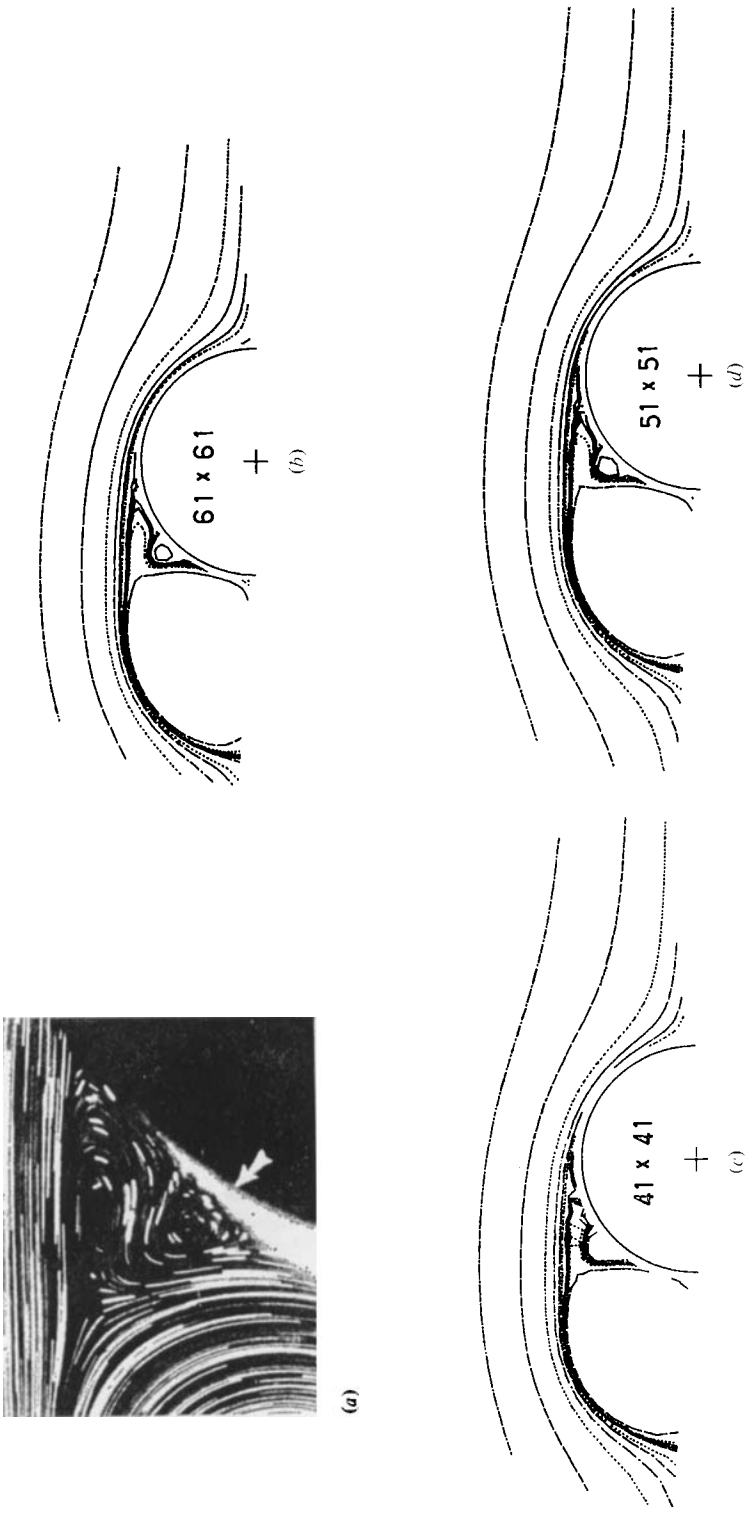

FIGURE 11. Comparison between numerical results and experimental visualization. (*a*) Flow visualization of Coutanceau & Bouard (1979), (*b, c, d*) streamlines for various grids: (*b*) 61×61; (*c*) 41×41; (*d*) 51×51.